



Laser induced graphene-based out-of-autoclave curing of fiberglass reinforced polymer matrix composites

Ruowen Tu^a, Tianqi Liu^a, Kelsey Steinke^b, Jalal Nasser^a, Henry A. Sodano^{a,b,c,*}

^a Department of Aerospace Engineering, University of Michigan, Ann Arbor, MI, 48109, USA

^b Department of Materials Science and Engineering, University of Michigan, Ann Arbor, MI, 48109, USA

^c Department of Macromolecular Science and Engineering, University of Michigan, Ann Arbor, MI, 48109, USA

ARTICLE INFO

Keywords:

Laser induced graphene
Joule heating effect
Out-of-autoclave curing
Fiberglass composites
Composite repair
Deicing

ABSTRACT

Fiberglass reinforced composites (FRCs) are traditionally cured in an autoclave or hot press, which are equipment known for their high energy consumption and their imposed constraints on the cured component sizes. Furthermore, current composite repair techniques usually require removing the composite part from service and using traditional composite fabrication methods to apply patches in a workshop. As an alternative to such techniques, this work presents a new out-of-autoclave (OoA) FRC curing method that relies on the Joule heating potential of transfer-printed laser induced graphene (LIG) interlayers. LIG is initially generated on polyimide substrates before then being transfer-printed onto fiberglass prepregs to form uniform surface coatings. The excellent electrical properties of the transfer-printed LIG are then exploited to in-situ cure fiberglass laminates via Joule heating effect. The LIG-coated FRCs cured through Joule heating (LIG-cured FRCs) is found to have a high degree of cure of 96%, comparable to oven-cured ones, while requiring 89.39% less specific energy. The mechanical properties of LIG-cured FRCs are measured and determined to match those fabricated using traditional approaches. Furthermore, LIG-coated fiberglass prepregs are shown capable of acting as in-situ bonding agents for the joining of two composite structures, which indicates its potential of composite repair through healing at the site of structure damage. Finally, the Joule heating effect of the LIG interlayers in cured FRCs is investigated and found to enable the fast and energy-efficient deicing of such composite structures. Therefore, the proposed OoA-curing method provides a simple and cost-efficient approach to manufacture FRCs with multifunctionality.

1. Introduction

Fiber reinforced polymer matrix composites (FRPMCs) possess a number of advantages over metallic and ceramic materials due to them being simultaneously strong, lightweight, corrosion resistant, tailorable, and easy to process [1,2]. As a result, FRPMCs have become increasingly popular in structural applications within the aerospace, automotive, and marine industries where lightweight and high strength materials are typically desired [3–5]. As the market for FRPMCs continues to grow, greater research focus has been dedicated to improving and optimizing their corresponding manufacturing procedures, especially with regards to the curing processes of their thermosetting polymer matrices. Traditionally, FRPMCs are cured in large autoclaves and under optimal conditions pertaining to cure pressure, temperature, and cycle, such that the resulting mechanical properties of the final product are maximized

[6–8]. However, the high energy consumption and low efficiency of autoclaves, along with their imposed restrictions on final part dimensions, have spawned interest in the development of more convenient and efficient out-of-autoclave (OoA) fabrication processes. Such manufacturing methods reduce acquisition capital and costs, are compatible with a wider range of tooling and materials and eliminate geometrical constraints on the final size of the structure [9–13]. Therefore, given these described advantages, it is important to develop new OoA curing methods and technologies that efficiently yield composite parts exhibiting excellent mechanical properties.

A primary focus in the development of new OoA curing techniques for composite materials is to enable high production rates. Recently, microwave methods have been suggested as efficient and cost-effective techniques for the OoA curing of composite materials [14–16]. Relative to conventional curing methods, microwave heating allows for faster

* Corresponding author. Department of Aerospace Engineering, University of Michigan, Ann Arbor, MI, 48109, USA.

E-mail address: hsodano@umich.edu (H.A. Sodano).

<https://doi.org/10.1016/j.compscitech.2022.109529>

Received 20 December 2021; Received in revised form 12 April 2022; Accepted 13 May 2022

Available online 18 May 2022

0266-3538/© 2022 Published by Elsevier Ltd.

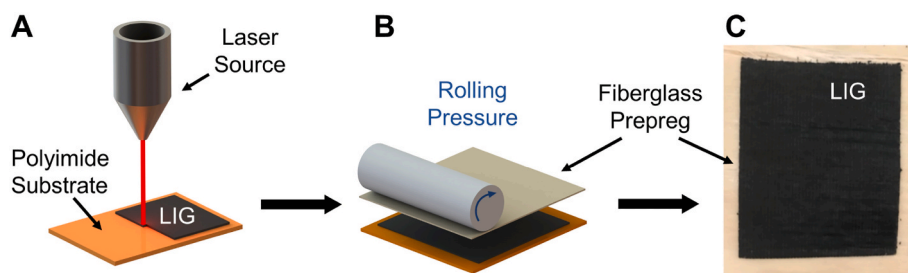


Fig. 1. Transfer-printing of LIG onto a fiberglass prepreg. A) Generation of LIG on polyimide substrate a CO₂ using a laser source. B) Transfer of LIG onto tacky fiberglass prepreg using a roller. C) Uniform LIG coating on fiberglass prepreg surface.

fabrication of fiber reinforced composites by relying on electromagnetic radiation to shorten curing cycles [14]. Kwak et al. used a Votsch Hephaistos microwave (VHM) system to cure carbon fiber reinforced epoxy prepreg composites at a 100% faster rate relative to a conventional oven curing technique, all while maintaining mechanical properties [17]. Li et al. also optimized the microwave curing process in order to minimize temperature gradients along the through-thickness direction of composite materials [18]. The modified vacuum assisted microwave curing technology relied on vacuum pipes and Fiber Bragg Grating sensors that allowed for efficient control over the power of magnetrons and subsequently yielded uniform temperature distributions during curing [18]. Although such an approach presents significant advantages related to improving cost-effectiveness and shortening curing cycles, the success of this method remains largely dependent on the dipolar properties of the cured materials [17], as the specific frequency of the microwave is required to be in tune with the unique characteristics of the cured material and process employed [19,20].

Due to the previously described limitations and challenges rising from microwave processing, great research interest has also been allocated to resistive and inductive curing methods. The majority of reported studies regarding such curing techniques investigate the potential of carbon nanotubes (CNTs) as electrically conductive heating elements in carbon fiber reinforced composite materials [15,21–23]. Both macroscale carbon fibers and CNTs are proven to be conductors of heat and electricity, making Joule heating an ideal approach for realizing the large scale OoA manufacturing of such composite materials [21]. Nguyen et al. investigated the potential of CNT buckypapers as Joule heating elements for the curing of carbon fiber reinforced bismaleimide matrix composites [22]. The thermally conductive CNTs were shown to enable energy-efficient and uniform heating throughout the composite laminate and induce curing. Xu et al. also demonstrated the potential for using CNT films to heat and cure fiberglass reinforced composites (FRCs) [15]. The employed curing process was found to consume about one seventh of the energy necessary for achieving similar results using a conventional oven curing process, thus highlighting the advantages of OoA methods over traditional ones. Nonetheless, CNT buckypaper fabrication remains a costly process due to the need for high-energy consumption synthesis methods such as chemical vapor deposition (CVD) [22]. Joule heating was also achieved in carbon fiber composites through the introduction of a multifunctional zinc oxide (ZnO) nanorod interphase [23]. The hydrothermally grown ZnO were found to yield great improvements in interlaminar Joule heating efficiency within the composite, acting as thermal traps and barriers that allow for greater heat retention. Nonetheless, this strategy is limited to composite materials consisting of conductive reinforcement such as carbon fiber, and cannot be extended to FRCs. Therefore, it remains necessary to develop OoA techniques that are compatible with electrically and thermally insulating composite materials such as FRCs.

Laser induced graphene (LIG) is a recently discovered, carbon-based nanomaterial that also exhibits excellent mechanical, thermal, and electrical properties like CNTs [24,25]. LIG can be described as a porous graphene material that is able to be generated on a number of

thermoplastic and thermosetting polymer substrates using a CO₂ infrared laser induction process in ambient conditions [26,27]. The morphology and physical properties of LIG can be easily tailored by controlling several induction parameters, primarily laser pulsing density, laser scanning speed and output power [28,29]. Given its previously mentioned exceptional properties, LIG has been successfully used in a wide variety of applications including microelectronics, solar cells, and biosensors [30–36]. Recent work has also shown that forest-like LIG can be transplanted off polyimide substrates and then attached to tacky prepreg surfaces using an optimized transfer-printing approach [37]. The embedded LIG interlayers were found to toughen carbon fiber composites, while also providing FRCs with self-sensing and damage detection capabilities under both quasi-static and dynamic loading conditions [37–40]. In addition, Smith et al. reported the thermal conductivity of LIG foam to be around $0.7 \text{ W m}^{-1} \text{ K}^{-1}$ [41], which is higher than the thermal conductivity of most bulk polymers ($0.1\text{--}0.5 \text{ W m}^{-1} \text{ K}^{-1}$) [42], and could be further increased by infiltrating polymer into the LIG foam. Therefore, the embedding of LIG interlayers into FRCs can provide their corresponding structures with unprecedented functionalities, all while improving the thermal conductivity and maintaining their mechanical properties. However, the Joule heating potential of LIG and its viability as an efficient and reliable OoA curing technique for FRCs remains unexploited.

The work presented here investigates the Joule heating effect of LIG for the OoA curing of FRCs. In this study, LIG was transfer-printed onto fiberglass prepreg surfaces and used as Joule heating elements that enable the in-situ curing of FRCs laminates in an energy efficient and size unconstrained manner. Temperature distribution within the laminate was monitored and tracked using thermal imaging and a thermocouple, while the final degree of cure of LIG-coated FRCs cured through Joule heating effect (LIG-cured FRCs) was measured using differential scanning calorimetry (DSC). The mechanical performance of both oven-cured and LIG-cured FRCs were evaluated and compared through tensile and three-point bend testing. In addition, LIG-coated FRCs exhibit multifunctionality through Joule heating effect. First, composite repair is a challenging work that usually requires the disassembly and removal of the damaged composite structure from service. LIG-coated FRC prepreps can be used as a cost-efficient in-situ bonding agent for in-situ composite repair, especially for delamination, which is one of the most common failure mechanisms of FRCs [43]. Second, with FRCs being increasingly used in wind turbine blades and airplane leading edges, significant challenges have arisen due to the low-temperature environments that these applications present. Specifically, the formation and accumulation of ice on FRC structures can considerably reduce their aerodynamic performance and cause for operation delays due to routine and time-consuming deicing [44]. With embedded LIG, FRCs are demonstrated to have the deicing capability through Joule heating, without any applied chemicals or external heat sources. Therefore, the proposed LIG interlayer enables the energy-efficient OoA-curing of FRCs, as well as the multifunctionality of the FRCs.

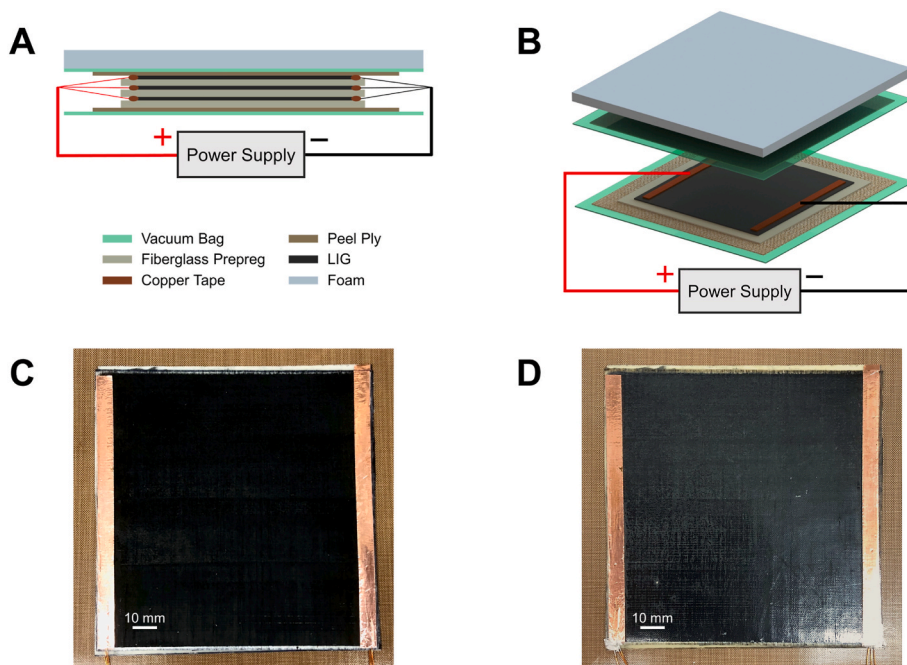


Fig. 2. Schematic of in-situ curing of LIG-coated fiberglass prepreg: A) Cross-section view; B) 3D view (only one ply is shown for better visualization). Images of a 3-ply LIG-coated FRC: C) Before in-situ curing; D) After in-situ curing.

2. Experimental methods

2.1. Transfer of LIG onto fiberglass surface

LIG was directly induced on Kapton® polyimide substrates (2 mil thickness) and then transfer-printed to the top surfaces of fiberglass prepreps. The LIG coating was initially generated using a 40 W CO₂ universal laser system (Epilog Zing 16) operated in raster mode at an

areal speed of 0.1 cm² s⁻¹, a pulsing density of 400 dots per inch (DPI), and a laser output power of 15% (Fig. 1A). The LIG was then transferred from the surface of the polyimide substrate to that of the pre-heated and tacky fiberglass prepreg (85 °C) by means of a manual roller transfer-printing process (Fig. 1B) that has been previously detailed by Groo et al. [37]. As shown in Fig. 1C, a successful transfer-printing process should yield a uniform and well-adhered LIG coating on the fiberglass surface. For characterization of the generated LIG in this work, Raman

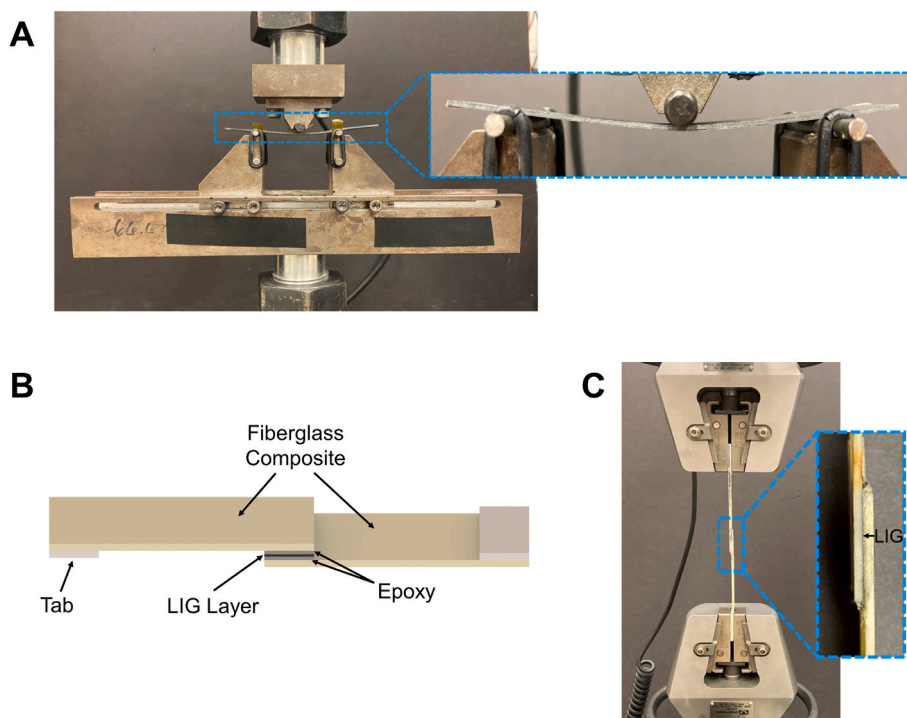


Fig. 3. A) Experimental setup for three-point bend testing. B) Schematic of single-lap joint test specimen with LIG layer bonded between two FRCs. C) Corresponding experimental setup.

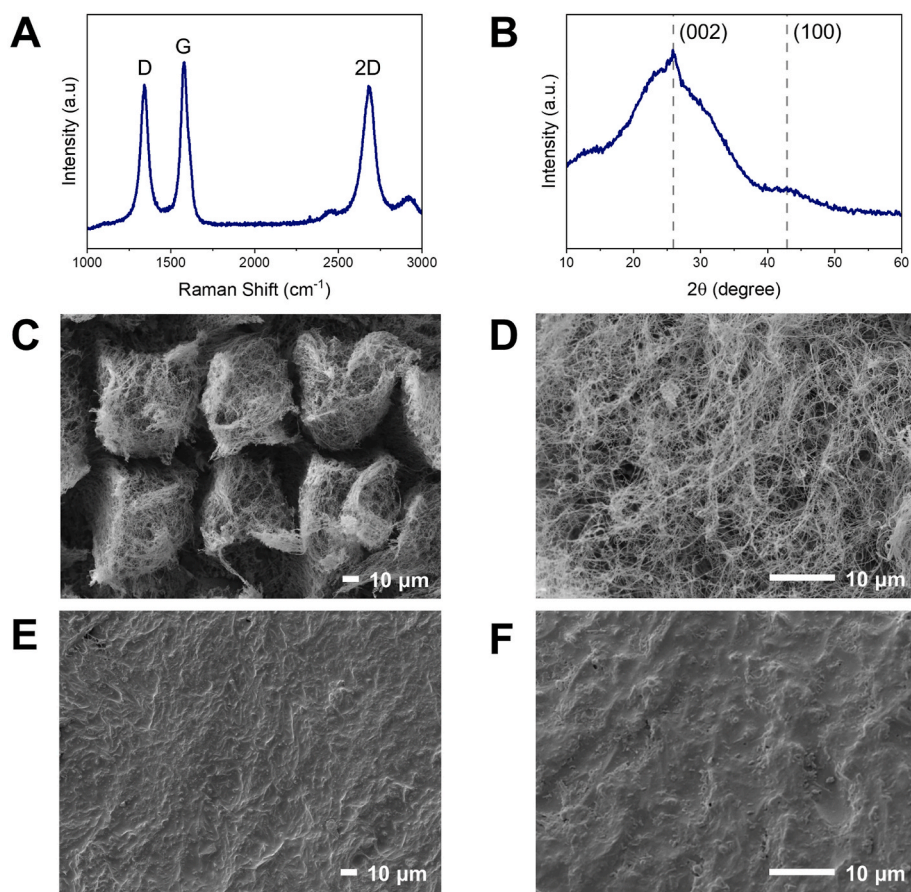


Fig. 4. A) Raman spectroscopy of LIG. B) XRD pattern of LIG. C & D) SEM images of LIG generated on polyimide substrate. E & F) SEM images of transfer-printed LIG that is embedded in cured FRCs.

spectroscopy was performed on LIG using a Renishaw inVia confocal microscope equipped with a 633 nm laser source, and X-ray diffraction (XRD) was performed using a Rigaku Ultima IV X-ray diffractometer with Cu K α radiation ($\lambda = 0.154$ nm).

2.2. In-situ curing process

In this study, oven-cured composites were fabricated using a traditional vacuum assisted resin transfer molding (VARTM) process, where the preform was cured for 2.5 h inside a hot press at 115 °C and 100 psi. In contrast, the LIG-cured composites were solely cured via the Joule heating effect of the transfer-printed LIG coatings (Fig. 2A and B). Initially, wire leads (33-gauge copper wire) were attached using conductive copper tape to each LIG-coated prepreg ply to act as electrodes, before then being connected to a DC power supply (Keysight E3649A). Fig. 2C and D are images of a 3-ply LIG-coated FRC before and after in-situ curing, respectively. Temperature distributions were monitored via infrared thermal imaging using a FLIR® ONE Pro thermal camera and a thermocouple that was placed on the top surface of the cured composites. The curing process was performed under vacuum while covering the preform with an insulating layer of foam that reduces heat loss and allows for uniform heating within the preform. The electrical energy consumption for the LIG-based curing method was measured by recording the power input and integrating the power over curing time, while the electrical energy consumption for the traditional oven/hot press curing method was measured using a clamp meter (FLUKE) and again calculated by integrating the power over curing time. Following curing, the degree of cure of both oven-cured and LIG-cured composites was analyzed using differential scanning calorimetry (Q2000 analyzer from TA Instruments) by applying a heating ramp from

0 °C to 250 °C at a rate of 5 °C min⁻¹. The degree of cure was calculated using the following relationship:

$$\alpha = \frac{H_T - H_r}{H_T} \times 100\% \quad (1)$$

where α is the degree of cure, whereas H_T and H_r are the total and residual heat of the complete exothermal reaction, respectively. Finally, LIG morphology was investigated pre-transfer and post-curing using a JEOL JSM-7800FLV field emission scanning electron microscope.

2.3. Mechanical testing

Tensile testing of oven-cured and LIG-cured composites were performed according to ASTM D3039. The cured tensile specimens consisted of 4 LIG-coated fiberglass plies stacked together in a $[\pm 45^\circ]_s$ sequence, and were cut to dimensions specified by the ASTM standard with a gauge length of approximately 250 mm. Woven fiberglass tabs were then bonded on both ends of the specimens using high shear strength epoxy (Loctite EA 9430™ Hysol). For each data set, 6 specimens were loaded using an Instron universal load frame (Model 5982) at a rate of 2 mm min⁻¹ until failure. The tensile chord modulus of elasticity was approximated according to the recorded stress-strain curves and within the 0.3% and 1% strain range.

The flexural properties of oven-cured and LIG-cured composites were also evaluated using three-point bend testing according to ASTM D790-17. The specimens consisted of 4 LIG-coated fiberglass plies stacked together in a $[\pm 45^\circ]_s$ sequence and were cut to dimensions specified by the ASTM standard with a gauge length of approximately 240 mm. As seen in Fig. 3A, 6 specimens of each data set were loaded in a three-point bending configuration using an Instron universal load

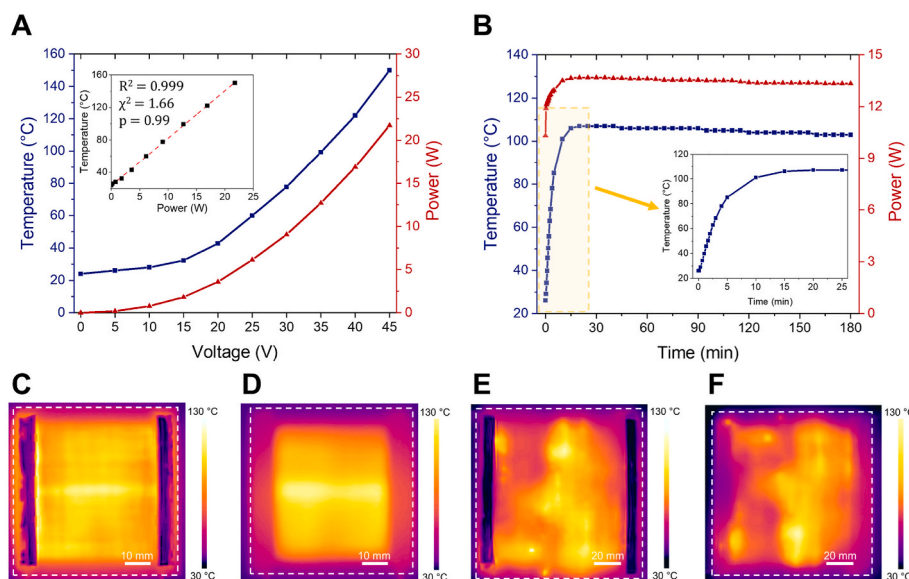


Fig. 5. A) Relationship between applied voltage and LIG-coated FRC temperature, and relationship between electrical power and LIG-coated FRC temperature. B) Temperature and electrical power profile during the LIG-based curing process. C) & D) Thermal imaging of top and bottom surfaces of a small LIG-coated FRC during LIG-curing. E) & F) Thermal imaging of top and bottom surfaces of a large LIG-coated FRC during LIG-curing.

frame (Model 5982) at a span-to-thickness ratio of 40:1 and a rate of 2 mm min^{-1} until failure. As per ASTM D790-16, the flexural strength and stiffness of the oven-cured and LIG-cured FRCs were calculated according to the secant method.

2.4. LIG-based composite bonding and repair

The potential of a single LIG-coated fiberglass prepreg as a Joule heating bonding agent for repair operations of composite materials was evaluated using single-lap joint shear test, according to ASTM D1002. Unidirectional FRCs were fabricated using a VARTM process and then cut to dimensions of 101.6 mm in length and 25.4 mm in width, before adhering woven fiberglass tabs to only one of their ends using a high shear strength epoxy (Loctite EA 9430™ Hysol). The prepared composite strips were then bonded to each other via the Joule effect of a unidirectional, LIG-coated fiberglass prepreg over a $12.7 \text{ mm} \times 12.7 \text{ mm}$ overlap shear area (Fig. 3B). Additional high shear strength epoxy was also applied to the shear area between the two composite panels to further reinforce the fabricated lap joint (Fig. 3B). These joints were cured at a temperature of $115 \text{ }^\circ\text{C}$ via the LIG coating acting as a Joule heating element by applying a current of 0.2 A for 2.5 h. The shear strength of the lap joints was finally measured in an Instron load frame at a crosshead control rate of 1.27 mm min^{-1} until failure (Fig. 3C). It should be noted that since the epoxy used in this test can be fully cured at room temperature after 5 days, LIG-cured lap joints were tested the same day after curing to show its reduction in curing time using the LIG coating.

2.5. LIG-based deicing

The deicing functionality of cured LIG-coated FRCs was demonstrated through two sets of experiments: one at room temperature, and the other at subfreezing temperature. For room temperature deicing, an ice cube (about 8 g) was placed on the LIG-coated FRC with a 40 V input voltage for Joule heating, and the time and energy to completely melt the ice were measured. The ice melting process was also compared to another ice cube placed next to the FRC without any additional heating. In addition, an ice cube was bonded to the surface of an LIG-coated FRC using additional water and then kept in a freezer at $-18 \text{ }^\circ\text{C}$ for approximately 20 h until the ice completely froze to the composite

surface. Subsequent the ice coated composite was removed from the freezer, the composite was placed on a ramp and applied a 40 V input voltage for Joule heating, to show the fast melting of the ice/composite interface for deicing. For subfreezing temperature deicing, due to the limitation of creating a subfreezing environment in the lab, a cold plate (VEVOR) with a constant surface temperature ($-20 \text{ }^\circ\text{C}$) was used to create a subfreezing substrate. An LIG-coated FRC was placed on the cold plate with an ice cube on top of it, and it was heated by applying a 60 V input voltage to melt the ice. For comparison, another ice cube was placed directly on the cold plate as a reference. To simulate a more realistic scenario, a thin layer of water was frozen on the LIG-coated FRC to form a layer of surface ice. The ice-coated composite was then placed on the cold plate, and heated by applying a 60 V input voltage. The time and energy consumption for deicing at subfreezing temperature were recorded.

3. Results and discussion

3.1. LIG characterization and Joule heating behavior

Raman spectrum of the LIG generated on the polyimide substrate is shown in Fig. 4A, where the typical D peak ($\sim 1350 \text{ cm}^{-1}$), G peak ($\sim 1580 \text{ cm}^{-1}$) and 2D peak ($\sim 2700 \text{ cm}^{-1}$) indicate that it has a graphitic structure [26,28,45]. Specifically, the 2D peak represents the second order of zone-boundary phonons, and a single sharp 2D peak suggests the formation of several layers of graphene in LIG, unlike bulk graphite [45]. Fig. 4B shows the XRD pattern of the generated LIG powder. The main peak at $2\theta = 25.9^\circ$, which corresponds to a spacing of $\sim 3.4 \text{ \AA}$ between the (002) planes of graphene [28], confirms the presence of a high degree of graphene in LIG. A relatively low intensity peak at $2\theta = 42.9^\circ$ is related to 2D in-plane symmetry (001) along the graphene sheets [28,46]. Therefore, both the Raman spectroscopy and XRD have verified a large amount of graphitic structure existing in LIG. Before lasering, the polyimide tape has a thickness of $65.2 \pm 3.0 \text{ }\mu\text{m}$ without the adhesive layer, while after lasering the thickness of polyimide is reduced to $40.5 \pm 1.2 \text{ }\mu\text{m}$ without the adhesive layer. This measurement indicates that 38 vol% of polyimide is used for carbonization and LIG formation. Based on additional weight measurement of the polyimide substrate before and after lasering, the calculated LIG weight conversion efficiency is about 20%, which means the weight of

the generated LIG is 20% of the weight loss of the polyimide. The Joule heating performance of LIG embedded in FRCs is largely dependent on the transfer-printing process and both the quality and uniformity of the final nanostructured coating. Initially generated on a polyimide substrate, LIG arrays consist of vertically aligned micro-pillars comprised of interlaced graphene fibers (Fig. 4C and D). The observed porous nanostructure of LIG is desirable as it can subsequently allow for easy resin infusion during curing once transfer-printed to fiberglass prepreg surfaces. Fig. 4E and F shows the LIG coating is completely embedded within the matrix and fully integrated into the composite structure following curing. It should be noted that the adopted LIG morphology has been studied and optimized in a previous study in order to allow for effective LIG transfer-printing, while simultaneously maintaining mechanical properties and introducing multifunctionality [37]. The sheet resistance of the LIG generated on the polyimide substrate is measured to be $65.9 \pm 7.6 \Omega/\text{sq}$ using a four-point-probe approach, while after transfer-printing the sheet resistance of the LIG-coated fiberglass prepreg is increased up to $178 \pm 37 \Omega/\text{sq}$, due to some loss of the conductive LIG remaining on the polyimide substrate. For LIG-coated FRC curing, the relationship between the applied voltage and both composite temperature and electrical power consumption were first defined and are shown in Fig. 5A. Initially, the Joule heating effect of the LIG yields a slow increase in temperature with increasing voltage, as the generated heat is quickly dissipated through the ambient environment. However, once the applied voltage is increased to 15 V or greater, the composite temperature is observed to quadratically increase up to a maximum of 145 °C. The observed temperature trend is also found to be in linear correlation with the electrical power consumption, where a linear fit applied in Fig. 5A shows a R^2 value of 0.999, a χ^2 value of 1.66, and a p-value of 0.99, which means this linear fit is a good prediction for the temperature. As recommended by the manufacturer, the LIG-based curing of an 8000 mm² FRC was performed at a temperature of 115 °C for approximately 2.5 h via LIG Joule heating by applying 35 V to the specimen through the wire leads. As seen in Fig. 5B, the LIG-based curing process necessitates approximately 15 min to reach the steady state curing temperature, as both heat generation and dissipation rates reach an equilibrium. It should be noted that although the input voltage is kept constant, the electrical power input is observed to slightly increase before reaching steady state temperature, which is due to the slight decrease in LIG's electrical resistance with increasing temperatures. A negative temperature coefficient of resistance (NTC) is commonly observed in carbon-based materials such as CNTs, carbon fiber, and LIG [33,47,48]. Once steady state is reached, no significant changes in temperature or power are observed for the entirety of the LIG-based curing process. Furthermore, thermal images of the top and bottom surface of a 70 mm by 70 mm LIG-coated composite during cure clearly show a sufficiently uniform temperature distribution within the center area of the specimen, whereas the edges experience lower temperatures due to the higher dissipation and lower LIG coverage (Fig. 5C and D). Nonetheless, temperature difference between the top and bottom surface is determined to be negligible, thus demonstrating a uniform temperature distribution in the through-thickness direction. However, due to the inevitable inconsistency of the manual roller pressing approach, the uniformity of the transfer-printed LIG cannot be guaranteed for samples larger than the roller width, resulting in an uneven temperature distribution (Fig. 5E and F). Thus, in order to provide a uniform heating, an automated roller pressing system with constant pressure, speed and temperature can be potentially used for large samples in the future. The energy consumption of the LIG-based curing process for an 11 g composite can be obtained by integrating the area under the electrical power input curve, which is calculated to be 145 kJ. In comparison, performing the process in a 16,129 mm² oven/hot press would consume 1441 kJ. Thus, the LIG-based curing consumes 89.3% less electrical energy compared to the traditional oven/hot press curing method. After testing three 3-ply LIG-coated FRP samples with different sizes (6.5 g, 11.0 g and 17.3 g weight, respectively), the average specific energy

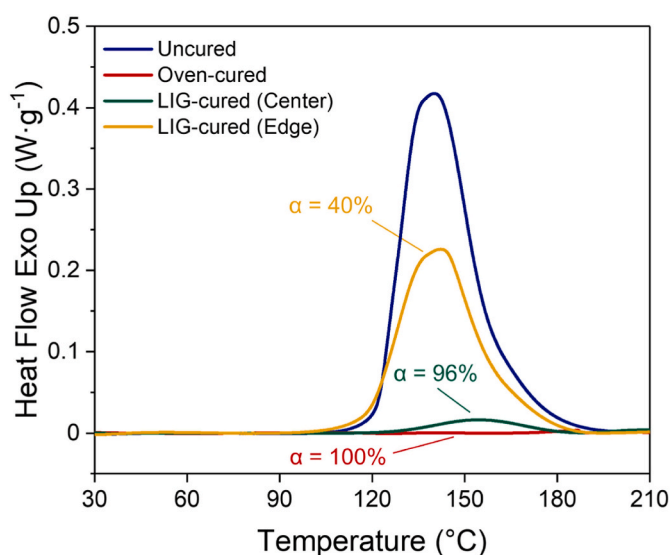


Fig. 6. DSC results and comparison between the degree of cure (α) of oven- and LIG-cured FRC specimens (DSC baselines are subtracted for better comparison).

consumption (energy consumption per unit weight of the composite) is calculated to be $15.17 \pm 2.42 \text{ kJ/g}$. In contrast, since the oven/hot press has a constant power output, the specific energy consumption for these three samples ranges from 83 to 221 kJ/g, which is still much higher than the LIG-based curing. These results suggest that the LIG-based curing approach is a more energy efficient alternative to oven curing process that also circumvents size constraints and can potentially yield similar structural performance.

3.2. Analysis of curing process

The effectiveness of the proposed LIG-based curing process was first evaluated by measuring the degree of cure using DSC (Fig. 6). The uncured fiberglass prepreg displays a broad exothermic peak from 100 to 190 °C corresponding to the heat emitted during matrix polymerization. After curing at 115 °C for 2.5 h, the center of LIG-cured FRCs displays a degree of cure of 96%, which is comparable to fully cured composites using an oven under the same conditions. Therefore, LIG joule heating can be exploited to yield a high degree of cure comparable to conventional methods in FRCs, while overcoming energy consumption concerns and size constraints. It can also enable the repair of composite structures without disassembly to allow curing in an oven or hot press. It should be noted that a slightly longer LIG curing time than the manufacturer recommendation can also be applied to further increase the degree of cure towards 100%, while keeping the energy consumption still much lower than traditional methods. However, the edges of the LIG-cured composites were found to exhibit a significantly lower degree of cure of 40%, primarily due to the previously discussed discrepancy in temperature distribution within the cured laminate, especially the low LIG coverage on the edges. Nonetheless, these edges consist of less than 10% of the total area of the composite and are usually discarded post-curing even in the case of oven-cured composites. Given the large contribution of the matrix to the overall structural performance of FRCs, the observed high degree of cure using the LIG approach is expected to translate into excellent mechanical properties.

3.3. Mechanical properties

The effect of the LIG-based curing process on the mechanical performance of FRCs is evaluated using tensile and flexural testing. In addition to improving energy efficiency and eliminating size constraints, it is critical for the proposed curing technique to yield a similar

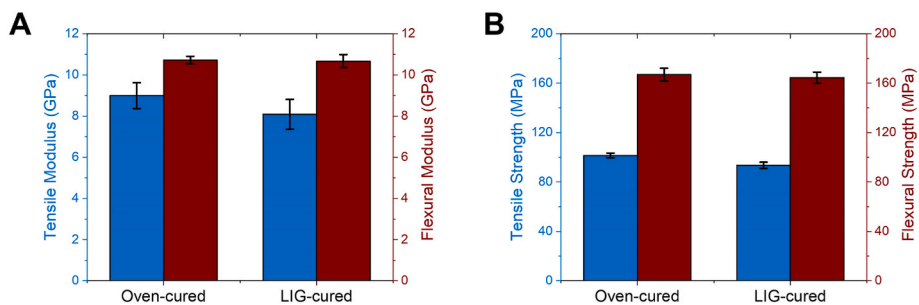


Fig. 7. A) Tensile chord modulus of elasticity and flexural modulus of oven-cured and LIG-cured FRCs. B) Tensile and flexural strength of oven-cured and LIG-cured FRCs.

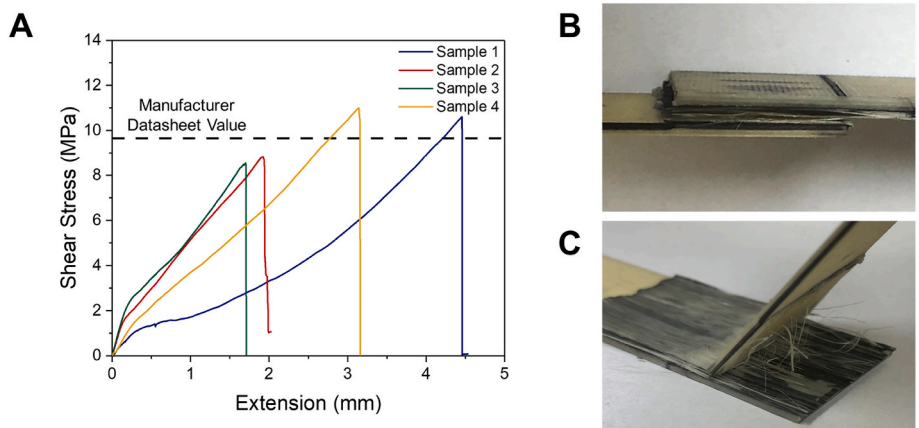


Fig. 8. A) Stress-extension curves of LIG-cured FRC single-lap shear strength tests. B & C) Cohesive failure mode of LIG-cured single-lap FRC specimens.

mechanical performance to that obtained using traditional oven-curing methods. As shown in Fig. 7A and B, the average tensile strength and chord modulus of elasticity of the LIG-cured specimens are found to be comparable to that of oven-cured specimens. Similarly, the average flexural strength and modulus of the LIG-cured specimens are observed

to match those of oven-cured specimens. These results were further validated through one-way analysis of variance (ANOVA) which concluded that there is no statistical difference in tensile modulus, flexural modulus and flexural strength between the LIG- and oven-cured FRCs specimens, respectively ($p > 0.05$). However, the test results show

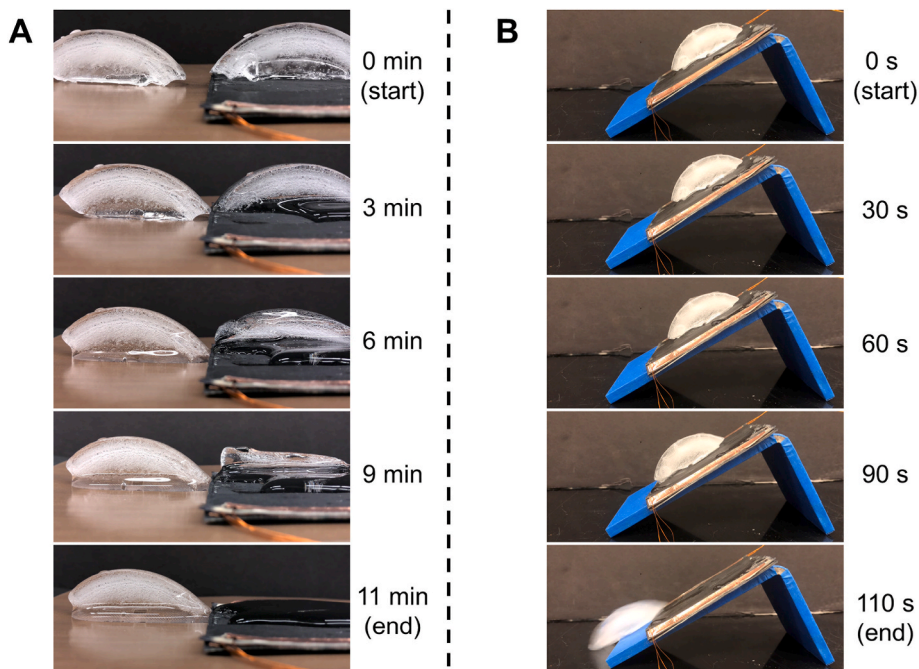


Fig. 9. Room temperature deicing: A) Melting of ice on FRC structure via LIG-based Joule heating. B) Deicing of FRC structure via LIG-based Joule heating.

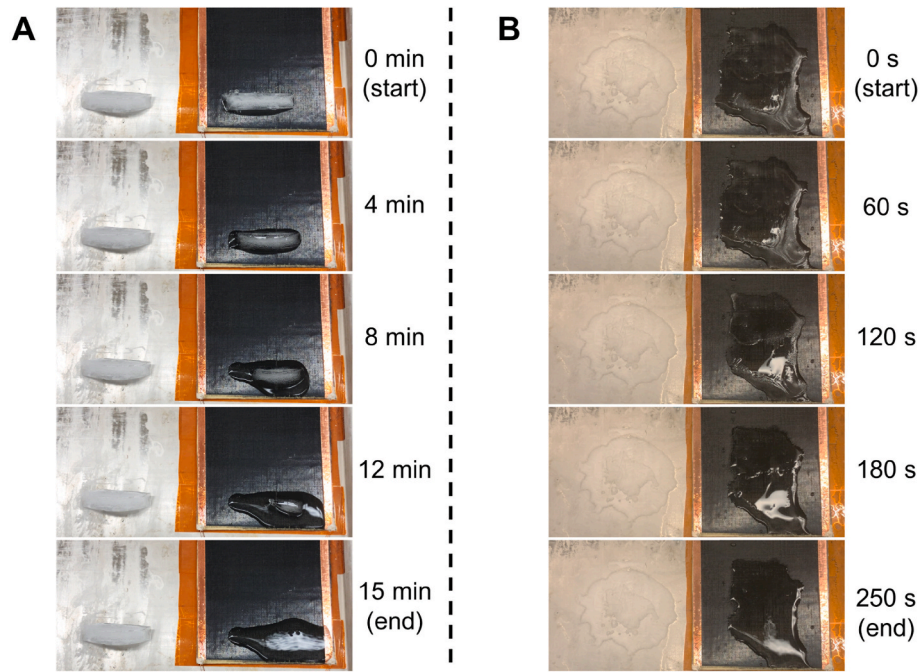


Fig. 10. Subfreezing temperature deicing: A) Melting of ice on FRC structure via LIG-based Joule heating. B) Deicing of FRC surface ice via LIG-based Joule heating.

some difference in tensile strength between the LIG- and oven-cured FRCs specimens ($p = 0.041$), where the tensile strength of LIG-cured specimens is 6.1% lower than that of oven-cured ones. This slight reduction in tensile strength might be caused by a higher possibility of voids forming during LIG-based in-situ curing, since no additional pressure was applied in this process. In general, the mechanical testing results confirm that the previously determined high degree of cure achieved using the proposed joule heating technique translates into excellent mechanical performance in FRC structures. It should be noted that the overall effect of LIG on both the in-plane and out-of-plane properties of FRCs has been extensively studied and shown to either improve or maintain the mechanical performance [37]. Therefore, it can be concluded that the LIG-based curing of FRCs is a reliable alternative to traditional oven-curing processes which allows for overcoming size constraints and reducing energy consumption while maintaining quality and mechanical performance for structural applications.

3.4. Bonding and repair performance of cured LIG-coated FRCs

In addition to enabling OoA curing, the Joule heating effect of LIG can also be exploited for the in-situ repair of locally formed cracks in FRC structural parts. In this case, LIG-coated fiberglass prepreps are used to bond two separate composite parts or to repair a formed crack directly on site, thus eliminating the need to remove the component from service. Here, the two composite parts are adhered in a lap joint configuration using high shear strength epoxy (Loctite EA 9430™ Hysol) and a LIG-coated fiberglass prepreg that acts as a Joule heating element. As seen in Fig. 8A, the average shear strength of these lap joints is determined to be 9.75 MPa, which is in agreement with that reported by the manufacturer for this epoxy in fiber reinforced composites [49]. Furthermore, Fig. 8B and C confirm that these in-situ cured lap joints exhibit cohesive failure at the level of the overlapping area, as both matrix residue and fiber bridging can be observed on both composite fractured surfaces. This failure mode is known to require greater fracture energy to occur than an adhesive one, thus further highlighting the high strength of the LIG-cured lap joints [50,51]. From this result it can be concluded that LIG-coated fiberglass prepreps can be used as Joule heating elements for the in-situ bonding or repair of composite material such that maintenance time and cost are reduced and the need for

removing damaged parts from service is eliminated.

3.5. Deicing performance of cured LIG-coated FRCs

In addition to the in-situ curing of FRCs through LIG-based Joule heating, the cured LIG-coated FRCs can also be used for self-deicing without requiring any chemicals or external heaters. Post-fabrication, LIG-coated composites are found to be electrically conductive which enables Joule heating once an electric current is supplied. The first set of demonstrations is room temperature deicing. As seen in Fig. 9A and Video S1, an electric power input of 17.5 W results in the complete melting of an 8.8 g ice cube in approximately 11 min (energy consumption 11.6 kJ), as the LIG-coated FRC reaches a steady state temperature of 121 °C. For reference, less than 50% of an ice cube of identical weight is observed to melt during a similar time period when kept at the same ambient conditions of 24 °C and 70% relative humidity. A further demonstration can be made by bonding the ice to the composite surface which is more consistent with traditional ice buildup on the surface. An 8.7 g ice cube is bonded to the surface of an LIG-coated FRC attached to a ramp, as explained in the experimental section, and an electric power of 17.5 W is applied to the LIG such that the ice/composite interface begins to melt and the ice begins slide off the surface under gravity after approximately 90 s, before completely sliding off after 110 s (Fig. 9B and Video S2). As the portion of ice that is directly in contact with the FRC surface begins to melt, a lubricated interface is formed, thus allowing the ice structure to easily slide off the FRC structure. The second set of demonstrations is subfreezing temperature deicing. By applying an electric power of 44.2 W to the LIG-coated FRC on top of the -20 °C cold plate, a 7.8 g ice cube placed on the FRC is completely melted in approximately 15 min (energy consumption 39.8 kJ), while on the left a reference ice cube directly placed on the cold plate does not display any shape change (Fig. 10A and Video S3). For a more realistic case, a thin layer of ice is frozen on the surface of the FRC that is placed on the cold plate, and a 44.2 W electric power is applied to the FRC for deicing (Fig. 10B). This results in a complete melting of the surface ice into water in about 250 s, consuming about 11.0 kJ electrical energy (Fig. 10B and Video S4). It should be noted that the power input and energy consumption for subfreezing temperature deicing are higher than room temperature deicing, because the cold plate absorbs a large

portion of the generated heat from the LIG. When compared to metal meshes and foils that are currently used in Joule heating-based deicing strategies, the embedded LIG coating can be seen as a lighter alternative that avoids degrading the mechanical properties of FRCs [15]. Given these observations, it can be then concluded that Joule heating via embedded LIG can enable fast and efficient strategies for the deicing of composite surfaces.

Supplementary data related to this article can be found at <https://doi.org/10.1016/j.compscitech.2022.109529>.

4. Conclusion

This research demonstrates the potential of LIG interlayers as Joule heating elements for OoA curing of FRCs. LIG was uniformly coated on fiberglass prepreg surfaces using a transfer-printing process before characterizing their Joule heating performance using thermal imaging and temperature measurements. The degree of cure of LIG-cured composites was measured using DSC analysis and was found to be comparable to oven-cured composites. Similarly, the tensile and flexural properties of LIG-cured composites were also determined to match those of reference oven-cured specimens, however the LIG-based curing process was found to consume 89.3% less electrical energy relative to the oven-curing process, thus acting as a more energy- and cost-efficient alternative while also eliminating any constraints on final part size. Furthermore, the use of LIG-coated fiberglass prepreg as a Joule heating element for successfully bonding two separate composite parts was demonstrated using single-lap joint shear strength testing. The described process can be used to simplify and accelerate repair processes in damaged composite parts and reduce equipment requirements. Once cured, LIG-based Joule heating was also shown to be capable of enabling the rapid deicing of structural FRCs operating in low temperature environments. Given the described advantages, the LIG's Joule heating effect shows great potential for further advancing the large-scale fabrication of commercial composites, the capability to repair structural damage and their integration in new applications.

CRedit authorship contribution statement

Ruowen Tu: Formal analysis, Validation, Writing – original draft. **Tianqi Liu:** Methodology, Validation, Formal analysis. **Kelsey Steinke:** Conceptualization, Methodology. **Jalal Nasser:** Conceptualization, Writing – original draft. **Henry A. Sodano:** Conceptualization, Supervision, Writing – review & editing.

Declaration of competing interest

The authors declare that they have no known competing financial interests or personal relationships that could have appeared to influence the work reported in this paper.

Acknowledgment

The authors gratefully acknowledge financial support for this research from the National Science Foundation under Grant # CMMI-1762369 and # EFRI-1935216.

References

- [1] K.J. Spoo, Corrosion resistance of various glass fiber reinforcements, in: *OnePetro*, 2009, in: <https://onepetro.org/NACECORR/proceedings/CORR09/All-CORR09/NACE-09327/128732>. (Accessed 16 November 2021).
- [2] J.M. Stickel, M. Nagarajan, Glass fiber-reinforced composites: from formulation to application, *Int. J. Appl. Glass Sci.* 3 (2012) 122–136, <https://doi.org/10.1111/j.2041-1294.2012.00090.x>.
- [3] United States Federal Aviation Agency, *Application of Glass Fiber Laminates in Aircraft*, U.S. Government Printing Office, 1964.
- [4] A. John, S. Alex, P. Scholar, A Review on the Composite Materials Used for Automotive Bumper in Passenger Vehicles, (n.d.) 4.
- [5] D.K. Rajak, D.D. Pagar, P.L. Menezes, E. Linul, Fiber-reinforced polymer composites: manufacturing, properties, and applications, *Polymers* 11 (2019) 1667, <https://doi.org/10.3390/polym11101667>.
- [6] F.Y.C. Boey, Simple autoclave systems for fibre reinforced composite components, *Polym. Test.* 8 (1988) 101–108, [https://doi.org/10.1016/0142-9418\(88\)90019-0](https://doi.org/10.1016/0142-9418(88)90019-0).
- [7] F.Y.C. Boey, Development of an autoclave curing system for fibre reinforced polymer composites, *Polym. Test.* 8 (1988) 375–384, [https://doi.org/10.1016/0142-9418\(88\)90041-4](https://doi.org/10.1016/0142-9418(88)90041-4).
- [8] F.Y.C. Boey, S.W. Lye, Effects of vacuum and pressure in an autoclave curing process for a thermosetting fibre-reinforced composite, *J. Mater. Process. Technol.* 23 (1990) 121–131, [https://doi.org/10.1016/0924-0136\(90\)90152-K](https://doi.org/10.1016/0924-0136(90)90152-K).
- [9] P. Hubert, T. Centea, L. Grunefelder, S. Nutt, J. Kratz, A. Levy, 2.4 out-of-autoclave prepreg processing, in: P.W.R. Beaumont, C.H. Zweben (Eds.), *Comprehensive Composite Materials II*, Elsevier, Oxford, 2018, pp. 63–94, <https://doi.org/10.1016/B978-0-12-803581-8.09900-8>.
- [10] D. Kim, T. Centea, S.R. Nutt, Out-time effects on cure kinetics and viscosity for an out-of-autoclave (OOA) prepreg: modelling and monitoring, *Compos. Sci. Technol.* 100 (2014) 63–69, <https://doi.org/10.1016/j.compscitech.2014.05.027>.
- [11] S.L. Agius, K.J.C. Magniez, B.L. Fox, Cure behaviour and void development within rapidly cured out-of-autoclave composites, *Compos. B Eng.* 47 (2013) 230–237, <https://doi.org/10.1016/j.compositesb.2012.11.020>.
- [12] M.A. Sunilpete, R.M. Cadambi, Development of cost effective out-of-autoclave technology – vacuum infusion process with tailored fibre volume fraction, *Mater. Today Proc.* 21 (2020) 1293–1297, <https://doi.org/10.1016/j.matpr.2020.01.165>.
- [13] Y. Yi, K. Saloniitis, P. Tsoutsanis, L. Litos, J. Patsavelas, Improving the curing cycle time through the numerical modeling of air flow in industrial continuous convection ovens, *Procedia CIRP* 63 (2017) 499–504, <https://doi.org/10.1016/j.procir.2017.03.167>.
- [14] N. Verma, R. Kumar, S. Zafar, H. Pathak, Vacuum-assisted microwave curing of epoxy/carbon fiber composite: an attempt for defect reduction in processing, *Manufacturing Letters* 24 (2020) 127–131, <https://doi.org/10.1016/j.mfglet.2020.04.010>.
- [15] X. Xu, Y. Zhang, J. Jiang, H. Wang, X. Zhao, Q. Li, W. Lu, In-situ curing of glass fiber reinforced polymer composites via resistive heating of carbon nanotube films, *Compos. Sci. Technol.* 149 (2017) 20–27, <https://doi.org/10.1016/j.compscitech.2017.06.001>.
- [16] B. Nuhji, T. Swait, M.P. Bower, J.E. Green, R.J. Day, R.J. Scaife, Tooling materials compatible with carbon fibre composites in a microwave environment, *Compos. B Eng.* 163 (2019) 769–778, <https://doi.org/10.1016/j.compositesb.2019.01.047>.
- [17] M. Kwak, P. Robinson, A. Bismarck, R. Wise, U. Middlesbrough, Curing of composite materials using the recently developed Hephaistos Microwave, in: *18th International Conference on Composite Materials*, 2011, pp. 1–6.
- [18] N. Li, Y. Li, X. Hang, J. Gao, Analysis and optimization of temperature distribution in carbon fiber reinforced composite materials during microwave curing process, *J. Mater. Process. Technol.* 214 (2014) 544–550, <https://doi.org/10.1016/j.jmatprotec.2013.10.012>.
- [19] J.J. Licari, D.W. Swanson, Chapter 4 - adhesive bonding processes, in: J.J. Licari, D. W. Swanson (Eds.), *Adhesives Technology for Electronic Applications*, second ed., William Andrew Publishing, Oxford, 2011, pp. 143–216, <https://doi.org/10.1016/B978-1-4377-7889-2.10004-X>.
- [20] H. Ku, F. Siu, E. Stores, J. Ball, A. Blichlau, Applications of fixed and variable frequency microwave (VFM) facilities in polymeric materials processing and joining, *Journal of Materials Processing Technology - J MATER PROCESS TECHNOL* 113 (2001) 184–188, [https://doi.org/10.1016/S0924-0136\(01\)00642-2](https://doi.org/10.1016/S0924-0136(01)00642-2).
- [21] I.M. Alarifi, Investigation the conductivity of carbon fiber composites focusing on measurement techniques under dynamic and static loads, *J. Mater. Res. Technol.* 8 (2019) 4863–4893, <https://doi.org/10.1016/j.jmtr.2019.08.019>.
- [22] N. Nguyen, A. Hao, J.G. Park, R. Liang, In situ curing and out-of-autoclave of interply carbon fiber/carbon nanotube buckypaper hybrid composites using electrical current, *Adv. Eng. Mater.* 18 (2016) 1906–1912, <https://doi.org/10.1002/adem.201600307>.
- [23] K. Kong, B.K. Deka, M. Kim, A. Oh, H. Kim, Y.-B. Park, H.W. Park, Interlaminar resistive heating behavior of woven carbon fiber composite laminates modified with ZnO nanorods, *Compos. Sci. Technol.* 100 (2014) 83–91, <https://doi.org/10.1016/j.compscitech.2014.06.006>.
- [24] A.K. Geim, Graphene: status and prospects, *Science* 324 (2009) 1530–1534, <https://doi.org/10.1126/science.1158877>.
- [25] M. Sang, J. Shin, K. Kim, K.J. Yu, Electronic and thermal properties of graphene and recent advances in graphene based electronics applications, *Nanomaterials* 9 (2019) 374, <https://doi.org/10.3390/nano9030374>.
- [26] J. Nasser, J. Lin, L. Zhang, H.A. Sodano, Laser induced graphene printing of spatially controlled super-hydrophobic/hydrophilic surfaces, *Carbon* 162 (2020) 570–578, <https://doi.org/10.1016/j.carbon.2020.03.002>.
- [27] J. Nasser, L. Groo, L. Zhang, H. Sodano, Laser induced graphene fibers for multifunctional aramid fiber reinforced composite, *Carbon* 158 (2020) 146–156, <https://doi.org/10.1016/j.carbon.2019.11.078>.
- [28] J. Lin, Z. Peng, Y. Liu, F. Ruiz-Zepeda, R. Ye, E.L.G. Samuel, M.J. Yacaman, B. I. Yakobson, J.M. Tour, Laser-induced porous graphene films from commercial polymers, *Nat. Commun.* 5 (2014) 5714, <https://doi.org/10.1038/ncomms5714>.
- [29] Y. Chyan, R. Ye, Y. Li, S.P. Singh, C.J. Arnsch, J.M. Tour, Laser-induced graphene by multiple lasing: toward electronics on cloth, paper, and food, *ACS Nano* 12 (2018) 2176–2183, <https://doi.org/10.1021/acsnano.7b08539>.
- [30] Z. Peng, R. Ye, J.A. Mann, D. Zakhidov, Y. Li, P.R. Smalley, J. Lin, J.M. Tour, Flexible boron-doped laser-induced graphene microsupercapacitors, *ACS Nano* 9 (2015) 5868–5875, <https://doi.org/10.1021/acsnano.5b00436>.

- [31] A. Nag, S.C. Mukhopadhyay, J. Kosel, Sensing system for salinity testing using laser-induced graphene sensors, *Sensor Actuator Phys.* 264 (2017) 107–116, <https://doi.org/10.1016/j.sna.2017.08.008>.
- [32] W. Ma, J. Zhu, Z. Wang, W. Song, G. Cao, Recent advances in preparation and application of laser-induced graphene in energy storage devices, *Mater. Today Energy* 18 (2020) 100569, <https://doi.org/10.1016/j.mtener.2020.100569>.
- [33] Z. Wan, M. Umer, M. Lobino, D. Thiel, N.-T. Nguyen, A. Trinchì, M.J.A. Shiddiky, Y. Gao, Q. Li, Laser induced self-N-doped porous graphene as an electrochemical biosensor for femtomolar miRNA detection, *Carbon* 163 (2020) 385–394, <https://doi.org/10.1016/j.carbon.2020.03.043>.
- [34] F. Wang, K. Wang, B. Zheng, X. Dong, X. Mei, J. Lv, W. Duan, W. Wang, Laser-induced graphene: preparation, functionalization and applications, *Mater. Technol.* 33 (2018) 340–356, <https://doi.org/10.1080/10667857.2018.1447265>.
- [35] L. Cao, S. Zhu, B. Pan, X. Dai, W. Zhao, Y. Liu, W. Xie, Y. Kuang, X. Liu, Stable and durable laser-induced graphene patterns embedded in polymer substrates, *Carbon* 163 (2020) 85–94, <https://doi.org/10.1016/j.carbon.2020.03.015>.
- [36] Y. Peng, W. Zhao, F. Ni, W. Yu, X. Liu, Forest-like laser-induced graphene film with ultrahigh solar energy utilization efficiency, *ACS Nano* 15 (2021) 19490–19502, <https://doi.org/10.1021/acsnano.1c06277>.
- [37] L. Groo, J. Nasser, L. Zhang, K. Steinke, D. Inman, H. Sodano, Laser induced graphene in fiberglass-reinforced composites for strain and damage sensing, *Compos. Sci. Technol.* 199 (2020) 108367, <https://doi.org/10.1016/j.compscitech.2020.108367>.
- [38] L. Groo, J. Nasser, D.J. Inman, H.A. Sodano, Transfer printed laser induced graphene strain gauges for embedded sensing in fiberglass composites, *Compos. B Eng.* 219 (2021) 108932, <https://doi.org/10.1016/j.compositesb.2021.108932>.
- [39] L. Groo, J. Nasser, D. Inman, H. Sodano, Damage localization in fiberglass-reinforced composites using laser induced graphene, *Smart Mater. Struct.* 30 (2021), 035006, <https://doi.org/10.1088/1361-665X/abdc0c>.
- [40] L. Groo, J. Nasser, D. Inman, H. Sodano, Fatigue damage tracking and life prediction of fiberglass composites using a laser induced graphene interlayer, *Compos. B Eng.* 218 (2021) 108935, <https://doi.org/10.1016/j.compositesb.2021.108935>.
- [41] M.K. Smith, D.X. Luong, T.L. Bougher, K. Kalaitzidou, J.M. Tour, B.A. Cola, Thermal conductivity enhancement of laser induced graphene foam upon P3HT infiltration, *Appl. Phys. Lett.* 109 (2016) 253107, <https://doi.org/10.1063/1.4972790>.
- [42] C. Huang, X. Qian, R. Yang, Thermal conductivity of polymers and polymer nanocomposites, *Mater. Sci. Eng. R Rep.* 132 (2018) 1–22, <https://doi.org/10.1016/j.mser.2018.06.002>.
- [43] R. Talreja, C.V. Singh, *Damage and Failure of Composite Materials*, Cambridge University Press, Cambridge, 2012, <https://doi.org/10.1017/CBO9781139016063>.
- [44] W.O. Valarezo, F.T. Lynch, R.J. McGhee, Aerodynamic performance effects due to small leading-edge ice (roughness) on wings and tails, *J. Aircraft* 30 (1993) 807–812, <https://doi.org/10.2514/3.46420>.
- [45] A.C. Ferrari, J.C. Meyer, V. Scardaci, C. Casiraghi, M. Lazzeri, F. Mauri, S. Piscanec, D. Jiang, K.S. Novoselov, S. Roth, A.K. Geim, Raman spectrum of graphene and graphene layers, *Phys. Rev. Lett.* 97 (2006) 187401, <https://doi.org/10.1103/PhysRevLett.97.187401>.
- [46] S. Dimovski, A. Nikitin, H. Ye, Y. Gogotsi, Synthesis of graphite by chlorination of iron carbide at moderate temperatures, *J. Mater. Chem.* 14 (2004) 238–243, <https://doi.org/10.1039/B311938F>.
- [47] A. Maffucci, F. Micciulla, A.E. Cataldo, G. Miano, S. Bellucci, Modeling, fabrication, and characterization of large carbon nanotube interconnects with negative temperature coefficient of the resistance, *IEEE Trans. Compon. Packag. Manuf. Technol.* 7 (2017) 485–493, <https://doi.org/10.1109/TCPMT.2016.2643007>.
- [48] M. Marengo, G. Marinaro, J. Kosel, Flexible temperature and flow sensor from laser-induced graphene, in: 2017 IEEE SENSORS, 2017, pp. 1–3, <https://doi.org/10.1109/ICSENS.2017.8234429>.
- [49] LOCTITE®, EA 9430 product description sheet. <http://tds.henkel.com/tds5/Studio/ShowPDF/243%20NEW-EN?pid=EA%209430&format=MTR&subformat=REAC&language=EN&plant=WERCS>, 2015. (Accessed 16 November 2021).
- [50] J. Nasser, L. Zhang, H. Sodano, Aramid nanofiber interlayer for improved interlaminar properties of carbon fiber/epoxy composites, *Compos. B Eng.* 197 (2020) 108130, <https://doi.org/10.1016/j.compositesb.2020.108130>.
- [51] J. Nasser, L. Zhang, H. Sodano, Laser induced graphene interlaminar reinforcement for tough carbon fiber/epoxy composites, *Compos. Sci. Technol.* 201 (2021) 108493, <https://doi.org/10.1016/j.compscitech.2020.108493>.